M&C 2017 - International Conference on Mathematics & Computational Methods Applied to Nuclear Science & Engineering, Jeju, Korea, April 16-20, 2017, on USB (2017)

Initial BWR Modeling Capability for MPACT

Brendan Kochunas[1], Daniel Jabaay[1], Andrew Fitzgerald[1], Thomas J. Downar[1], Scott Palmtag[2]

[1]*Department of Nuclear Engineering and Radiological Sciences*
University of Michigan, Ann Arbor, USA, bkochuna@umich.edu, djabaay@umich.edu, apfitzge@umich.edu, downar@umich.edu
[2]*Core Physics Inc. Cary, NC, USA, scott.palmtag@corephysics.com*

Abstract - *In this paper we present the recent advances in MPACT for modeling Boiling Water Reactors. The new features of the VERA input are briefly described. The approach to the general geometry meshing algorithm is based on the use of planar graphs and algorithms for computing the minimum cycle basis of the graph. The visualization capability for the general geometry uses a Delauney triangulation algorithm to construct the mesh points for VTK. The BWR capability based on these algorithms allows for the modeling and analysis of (i) narrow and wide inter-assembly gaps, (ii) channel boxes with rounded corners, (iii) cruciform control blades. Models of Peach Bottom Unit 2 cycle 1 lattices are developed in VERA for MPACT and KENO models are developed to provide reference solutions. The solutions of the two codes are compared and the average of the differences over the 6 lattices had a Δk of 97 pcm for the unrodded cases and 199 pcm for the rodded cases. The average pin power RMS was 0.24% and 0.28% for the unrodded and rodded cases, respectively. The average maximum difference was 0.46% for the unrodded cases and 0.90% for the rodded case. The BWR capability is also demonstrated for a variety of problems including: a 3-D control cell of "GE-12 like" assemblies with a partially inserted control rod, and a 2-D whole-core beginning of life state for Peach Bottom Unit 2.*

I. INTRODUCTION

MPACT [1] is the primary pin-resolved deterministic neutronics capability within VERA-CS [2], the core simulator being developed within CASL [3]. The extension of VERA-CS to model BWRs was a priority for Phase II of CASL.

There are currently 100 operating commercial power reactors in the US. Sixty-five of these are PWRs and 35 are BWRS. All of the BWR reactors in the US were designed and built by General Electric (GE). However, there are now three different fuel vendors that supply BWR fuel: Global Nuclear Fuel, Areva, and Westinghouse.

Each BWR fuel vendor has a slightly different assembly design. Some of the defining neutronics characteristics of a BWR compared to a PWR include the presence of a channel box around the fuel pins to isolate the void within each bundle, and a large water channel in the fuel pin lattice to assist in neutron moderation at high void conditions. Additionally, the first commercial reactors started with 7x7 fuel designs, but reactors have transitioned to more economical designs that use 8x8, 9x9, and 10x10 fuel. All BWRs in the US are currently using 10x10 fuel designs, but some international reactors still use 9x9 designs. There are also several other minor differences in the channel box design between modern and historical designs and vendors; such as "thick-thin" channel boxes and channel boxes with thick corners. Some of the modern and historical designs of various bundles are illustrated in Fig. 1.

Another distinguishing feature of a BWR core is the control blade design. Rather than having the rodlets of the control rod inserted into guide tubes in the assembly as in a PWR, the control blade is a large cruciform that is inserted between neighboring assemblies as shown in Fig. 2.

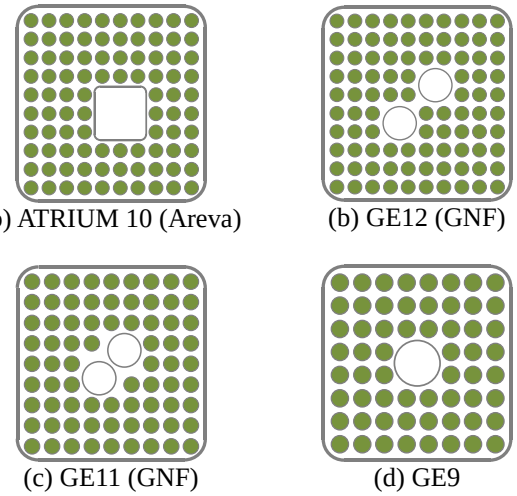

(b) ATRIUM 10 (Areva) (b) GE12 (GNF)

(c) GE11 (GNF) (d) GE9

Fig. 1. Illustrations of various BWR assembly designs.

In a BWR, the assembly pitch is also about 3/4 that of a PWR, and the number and arrangement of the assemblies within the core also differs from a PWR. At the core level, BWR assemblies are arranged in different rotational orientations around a control rod in a control cell as shown in Fig. 2. Finally, the operating conditions within a BWR are significantly different than in a PWR. BWRs operate at much lower pressure relative to a PWR, and boiling occurs in the pressure vessel, rather than in a steam generator as in a PWR.

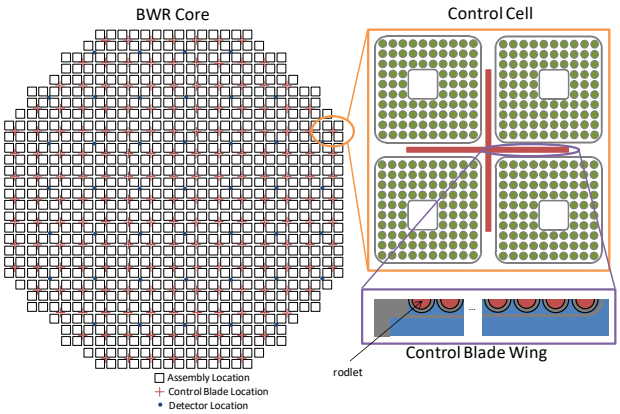

Fig. 2. Illustrations of a BWR core, control cell, and control blade wing.

The remainder of this paper is organized as follows: Section II provides the details of the newly implemented modeling capability, Section III presents some verification comparing MPACT results to KENO [4] results for lattice designs from Peach Bottom Unit 2 cycle 1, Section IV illustrates some additional features. Finally, Section V provides the conclusions and future work.

II. SUMMARY OF BWR CAPABILITY

The initial BWR modeling capability in MPACT includes the following features:

- Channel box with rounded corners
- Wide and narrow gaps on the outside of the channel box
- Ability to specify different void/density inside and outside the channel box
- Original Equipment Manufacturer (OEM) control blade design
- Large water rods that occupy 2x2 pin cells

The majority of the challenges in developing the initial BWR capability in MPACT involved modification of the input processing, model setup, and meshing. Since MPACT uses the method of characteristics (MOC) [1] for its transport solution algorithm, the actual neutron transport solver required no modification.

We note here that when we refer to the "meshing" process, our definition includes the steps that are necessary not only to establish a spatial discretization for the flat source region mesh required by the MOC implementation, but also the computation of the characteristic ray segments strictly required for MOC. Additionally, in some cases MOC based neutron transport codes may need modification to the ray tracking algorithm for changes made to the spatial mesh depending on the implementation. In MPACT, however, the existing MOC tracking algorithm is quite general, thus no modification to MPACT's tracking was required for the present work.

The modifications made to MPACT to incorporate the BWR features fall into roughly four categories:

- Input processing for new geometry features
- Addition of new more general geometry models/objects
- Automated meshing of the new general geometry
- Visualization of the new geometry and mesh

The details of the work performed in each of these categories are described in the following subsections.

1. VERA Input

Several aspects of BWR design required additions to the VERA input specification and processing. The vast majority of BWR geometry can be input in the same way as a PWR. For instance, a BWR still has an assembly map, which is made of lattices and pin cells, etc. However, as noted in Section 1, the principal differences arise for the following distinguishing BWR features: control blade, channel box, wide and narrow gap distance, 2-D void map, and large water rods. To best demonstrate the VERA input the example of a Peach Bottom lattice [6] with a control blade is shown along with the geometry in Fig. 3.

```
[ASSEMBLY]
  npin   8
  ppitch 1.6256   ! pin pitch - does not include channel gaps

!*** 80 mil design
  gap    0.9525 .47498   ! wide and narrow channel gap (cm)
!            material thickness inside-corner-radius (not used)
  channel_box  zirc4   0.2032         0.9652           0.0 0.0

  lattice LAT1
    2 1 1 1 1 1 1
    1 1 1 2 1 1 1
    1 1 2 2 2 2 1
    1 2 2 2 2 2 1
    1 1 2 2 2 2 1
    1 1 2 2 2 1 1
    1 1 1 1 1 1 1

[CONTROL]
  title "GE OEM Control Blade"
  npin 8
  stroke  365.76 48    ! 6in step size and 48 steps

  mat ss304 8.0
  mat b4c   1.74

  cell TUBE 0.17526 0.23876 / b4c ss304  ! BWR Blade rodlet

!       ntube     span    th       rad     sheath    wing    mat
  blade 21 TUBE 12.3825 0.79248 0.39624 0.14224  1.98501  ss304

!*** TUBE must be included in map, or it will be excluded from
!*** from the input
  rodmap  EMPTY
     TUBE
     - -
     - - -
     - - - -
     - - - - -
     - - - - - -
     - - - - - - -
     - - - - - - - -

  axial BLADE 0.0 EMPTY 1.0
```

Fig. 3. Example of VERA input for a BWR lattice

In addition to the new reactor components, the input processing in MPACT also automatically ro-tates the geometry given the location of the lattice in the core, so that the user is only required to input the geometry in a single orientation.

2. General Geometry Meshing Algorithm

MPACT represents components of the mesh with several data structures that parameterize the component features, rather than using a completely generic structure that would just list spatial coordinates for vertices and associated connectivity information. At the finest level there is the MOC flat source region (FSR) mesh. The mesh "above" the FSR mesh is the cross section (XS) mesh, contains one or more flat source regions. A set of XS meshes then comprise a pin cell mesh. The rest of the structures are fairly intuitive as they are based on reactor geometry constructs (e.g. assemblies).

The new meshing capability was implemented at the pin cell level, namely the geometry that is describable within a pin cell is now much more general. Circles, oriented bounding boxes, and lines can be placed arbitrarily within the pin cell mesh bounding box. The meshing algorithm then constructs a 2-D planar graph from the segments formed by the intersection of all the geometry objects. The points resulting in the unique closed volumes are determined by constructing the minimal cycle basis of the graph [7]. In graph theory, the definition of a cycle is similar to that of a polygon. For a graph made of vertices and edges, a cycle is a set of vertices whose edges are connected such that one may at any vertex in the set and traverse a continuous path back to the starting vertex. The cycle basis of a graph is essentially a set of cycles, that when combined produce a graph. The minimal cycle basis is the set of unique cycles in a graph such that each cycle in the set is a fundamental cycle (contains only one cycle) and there are no duplicate cycles.

After the minimal cycle basis is determined each cycle is converted to a newly implemented polygon primitive upon which the ray tracing is performed. The algorithm for the general geometry meshing process is illustrated in Fig. 4 and is given by the following procedure:

1. Determine intersections of geometry by consecutively overlaying geometry objects (e.g. circles, oriented bounding boxes, and lines).
2. Store intersections and segments in a planar graph.
3. Compute the minimal cycle basis of the planar graph in (2) to determine the XS mesh regions.
4. Intersect lines and subdivide XS mesh regions based on meshing parameters for each planar graph corresponding to each XS mesh region.
5. Compute the minimal cycle basis of the XS mesh region to obtain the flat source region mesh within that XS Mesh region
6. Repeat steps 4 and 5 until all XS mesh regions have been processed.

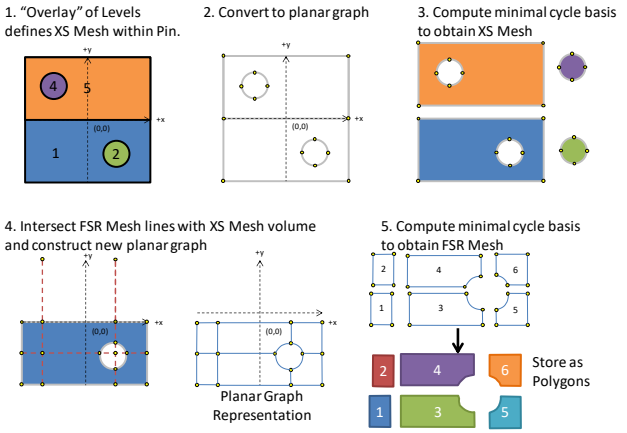

Fig. 4. General geometry MOC meshing algorithm.

Several complexities arise in this algorithm beyond those typically expected (e.g. removal of duplicate points, intersection of multiple segments at one point) that require special treatment. The additional complexities arise from the need to treat quadratic edges and the identification of "annular" volumes. This problem is particularly challenging when computing the volumes of the individual flat source regions.

3. Visualization of Geometry and Mesh

MPACT is capable of exporting its mesh to a VTK legacy file [8] that is viewable in VisIt [9] or similar programs.

Since VisIt does not support quadratic surfaces, although these are implemented in VTK, an extra step is involved to visualize the flat source regions from MPACT. Namely the polygons, from the 2-D MOC mesh are extruded axially, and then the quadratic surfaces are replaced by linear approximations, generally 32 points equally distributed in 2π are used. Duplicate points occurring at vertices shared between polygons are also removed.

This final list of points is then converted to a set of closed volumes where the connectivity of the points is determined from a Delaunay triangulation.

The Delaunay triangulation algorithm in MPACT is based on the sweep line algorithm [10], but is slightly modified to account for concentric rings. The whole process of model development and verification from input to visualization of the model is illustrated in Fig. 5.

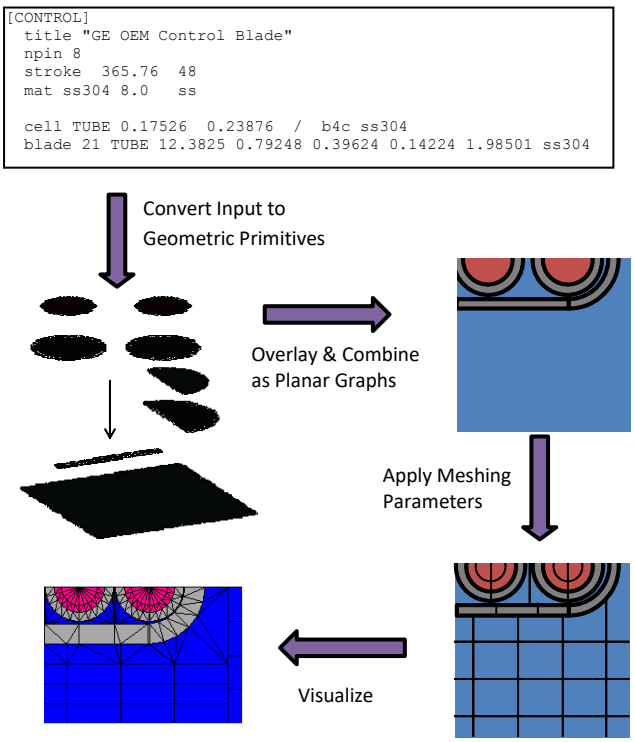

Fig. 5. Process of BWR model development and visualization.

III. COMPARISONS OF MPACT AND KENO

To verify the new modeling capability, several lattices from the Peach Bottom Unit 2 cycle 1 specs [6] were developed for MPACT using the VERA input. Separate models were also developed for KENO [4] to provide a reference solution. Additionally, a 3-D single assembly model was also developed and simulated with multiple control rod positions to verify the 3-D control rod positioning.

1. Comparisons of 2-D Peach Bottom Lattices

The MPACT models for the various Peach Bottom lattices are shown in Fig. 6. The bundles were simulated at hot zero power (HZP). This consisted of having all material temperatures at 600 K, and the water density was 0.736690 g/cc. The MOC discretization of the MPACT models used 0.01 cm spacing, 16 azimuthal angles and 2 polar angles per octant with the Cheybyshev-Yamamoto quadrature.

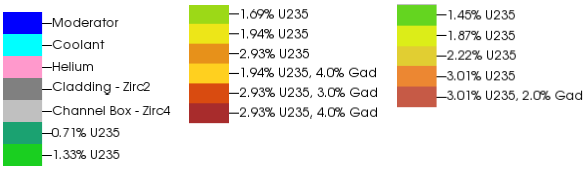

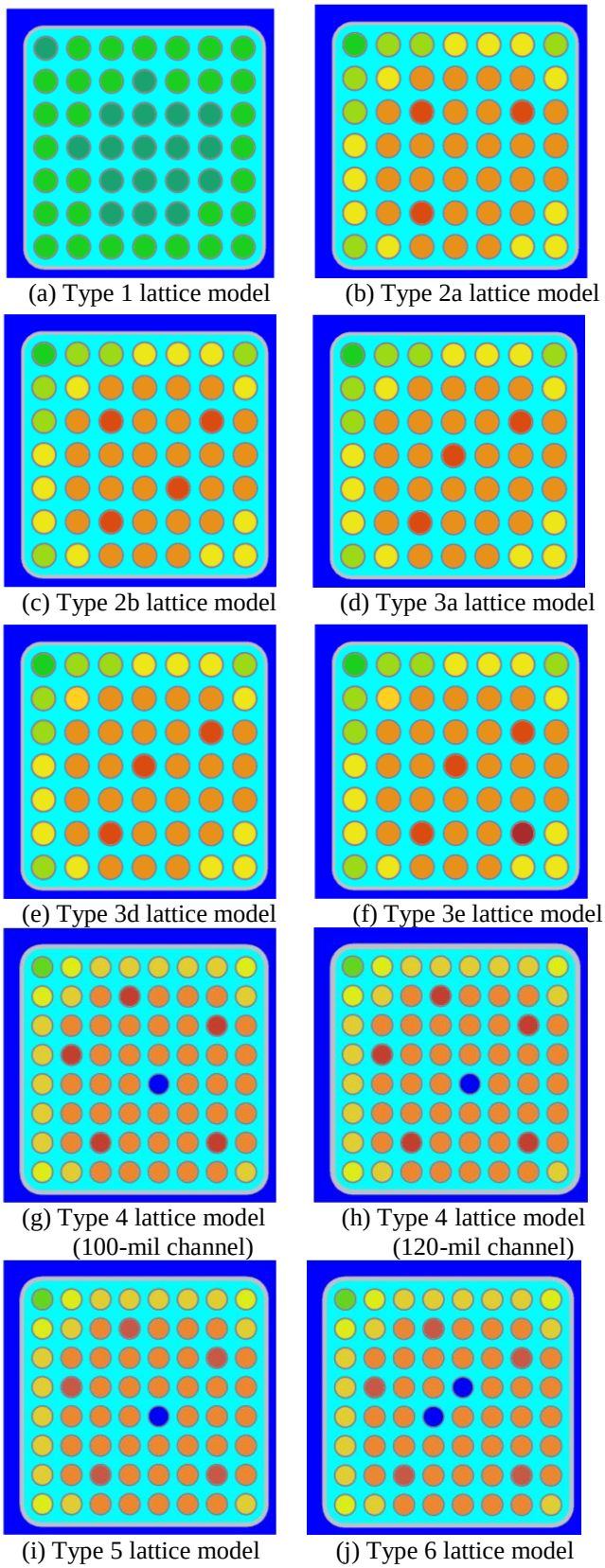

Fig. 6. Selected Peach Bottom lattice models for MPACT.

For MPACT, a new cross section library with 252 groups based on ENDF/B-VII.0 data [11] was used. P2 scattering was also used. KENO performed a continuous energy calculation with ENDF/B-VII.0 cross sections; simulating 2,000 active cycles, and 100 inactive cycles with 500,000 particles per cycle.

The comparisons of the results are given in Table 1 for the unrodded cases, and Table 2, for the rodded cases. For all cases, the uncertainty reported by KENO for kinf was < 3 pcm, and < 0.05% for any relative fission rate value.

Overall, these results show good agreement, however they also suggest some room for improvement. Previous comparisons of MPACT with KENO for PWR lattices [12] had differences approximately half of what is observed in the Peach Bottom comparisons. There also appears to be a consistent bias of approximately -100 pcm to -200 pcm for the unrodded and rodded cases respectively.

Table I. MPACT and KENO comparisons for unrodded Peach Bottom lattices at HZP

Lattice Type	Keno k_{inf}	MPACT Δk_{inf} (pcm)	Max Diff of Fiss Rate	RMS of Fiss Rate
1	1.05393	-20	0.28%	0.12%
2a	1.14621	-112	0.55%	0.30%
2b	1.10536	-127	0.53%	0.31%
3a	1.15548	-214	0.54%	0.28%
3d	1.09254	-125	0.57%	0.32%
3e	1.04024	-127	0.62%	0.34%
4 100mil	1.10087	-90	0.45%	0.24%
4 120mil	1.09890	-96	0.44%	0.23%
Type 5	1.11378	-90	0.48%	0.23%
Type 6	1.11257	-130	0.43%	0.22%

Table II. MPACT and KENO comparisons for rodded Peach Bottom lattices at HZP

Lattice Type	Keno k_{inf}	MPACT Δk_{inf} (pcm)	Max Diff of Fiss Rate	RMS of Fiss Rate
1	0.78854	-194	0.57%	0.20%
2a	0.90238	-205	0.81%	0.30%
2b	0.85967	-213	0.88%	0.32%
3a	0.89650	-213	0.79%	0.30%
3d	0.87656	-211	0.85%	0.31%
3e	0.81708	-204	0.96%	0.35%
4 100mil	0.87627	-177	1.03%	0.28%
4 120mil	0.87370	-177	0.90%	0.25%
Type 5	0.88651	-182	0.99%	0.28%
Type 6	0.88728	-250	0.94%	0.26%

2. Comparisons of 3-D Peach Bottom Assembly

A set of 3-D rodded assembly cases were run in MPACT and continuous energy KENO for comparison and verification. The type 1 lattice shown in Fig. 6 was expanded to a full 3-D assembly. The model specifies a lower water reflector, lower core plate, lower tie plate, fuel stack, upper gas plenum, spacer grids, upper tie plate, upper core plate and the control blade. The simulated conditions correspond to hot zero power.

As specified in [6], the control blade notches are 3 inches, and the drive mechanism only moves the blades in 2 notch intervals. Therefore, the cases were run with the control blade at 0, 12, 24, 36, and 48 steps withdrawn, with 48 being the fully withdrawn position. The MPACT model is shown Fig. 7.

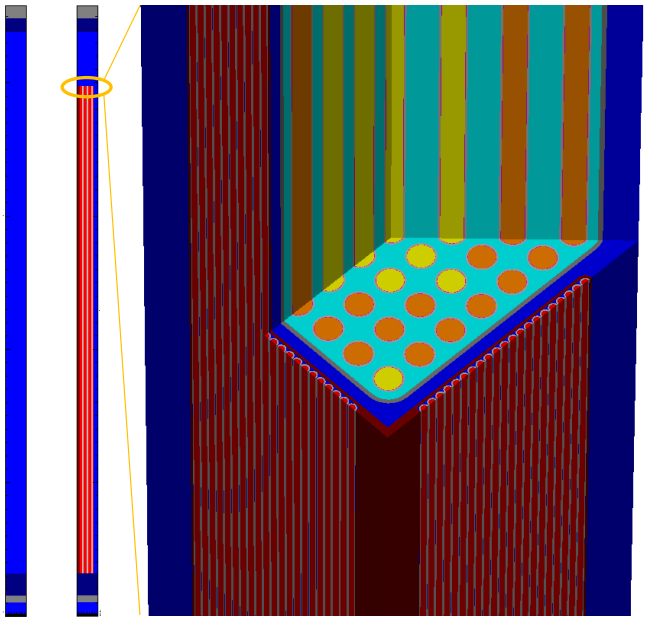

Fig. 7. MPACT model of Peach Bottom Unit 2 Cycle 1 Type 1 Assembly with partially inserted control blade

The MPACT cases used the new 51-group libraries also documented in [11]. The MOC discretization was 0.01 cm, 8 azimuthal, and 2 polar angles per octant. Once again the Cheybyshev-Yamamoto angular quadrature was used. These models were also simulated with TCP0, rather than P2 which was used for the lattices. Axially the model is discretized into 79 planes with 5.08 cm planes for the fuel.

The KENO models used 5 million particles per cycle and simulated 500 inactive cycles and 2000 active cycles. The results had a maximum statistical uncertainty of 0.7 pcm on k_{eff}. The uncertainties in the relative pin powers computed from KENO were < 0.20% for the fully inserted case and fully withdrawn cases. For the partially inserted cases, the statistics of the pins in the rodded regions were very large although disagreement between the MPACT and KENO did increase appreciably in these regions.

The results of the comparison between MPACT and KENO are given in Table III.

Table III. MPACT and KENO comparisons for Type 1 assembly for different rod positions at HZP

Rod Position (steps)	Keno k_{inf}	MPACT Δk_{inf} (pcm)	Max Diff of Fiss Rate	RMS of Fiss Rate
0	0.78549	-157	0.58%	0.26%
12	1.00887	117	0.67%	0.20%
24	1.03905	-33	0.74%	0.23%
36	1.04657	-59	0.76%	0.24%
48	1.04933	-78	0.74%	0.24%

In these models we see slightly increased differences compared to the 2-D lattices. The differences are bounded by a 157 pcm difference in reactivity, 0.74% maximum difference in the relative fission rate and 0.26% RMS.

Overall these differences are still quite good, although they are slightly increased over the 2-D lattices in terms of the fission rate distributions. This is not surprising given that the group structure and scattering order are reduced, and that the model has a partially inserted control rod.

Work is still ongoing to generate a BWR library for MPACT, and this may help to improve some of the differences observed in these results. It is known that the resonance integrals in the current library are generated with heterogeneous 2-D PWR pin cells with different fuel to moderator ratios and this might also be contributing to the observed differences. Furthermore, mesh sensitivity has yet to be performed in the inter-assembly gap regions and in the control blade, so it is assumed that this may also account for some of the differences. Nonetheless, for the present objectives in CASL to demonstrate the capability to model BWR geometry, these results provide sufficient verification to meet this objective.

IV. DEMONSTRATION PROBLEMS

To further assess the BWR capability in MPACT some additional demonstration problems were simulated. As a demonstration, no reference solution for these models exists. The purpose of the demonstration is to verify that other modeling capability exists and to evaluate the overall performance of MPACT for larger BWR models. The demonstration problems included a 2-D full core Peach Bottom Unit 2 model for the beginning of cycle 1 at cold zero power (CZP), and a 3-D "GE-12 like" assembly with vanished rods and axial blankets in a control cell.

1. 3-D BWR Control Cell

The 3-D bundle design was adapted from the fuel loading pattern specification of an Atrium-10 design given in [13], and the large water rod inner diameter is chosen to preserve this bundle fuel to moderator ratio. The 3-D model was also given 6-inch natural uranium blankets at the top and bottom and the channel box and an upper plenum region were defined with dimensions consistent with what was given in [6]. Part length rods, homogenized grid spacers, tie plates, axial reflectors and core plates based on [6] were also incorporated into the model. The images of this model are shown in Fig. 8. The fast and thermal flux are shown in Fig. 9.

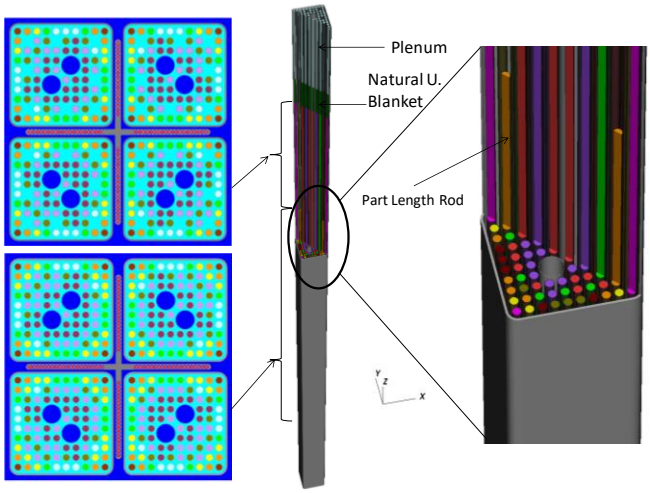

Fig. 8. Visualization of MPACT geometry for 3-D BWR assembly and power.

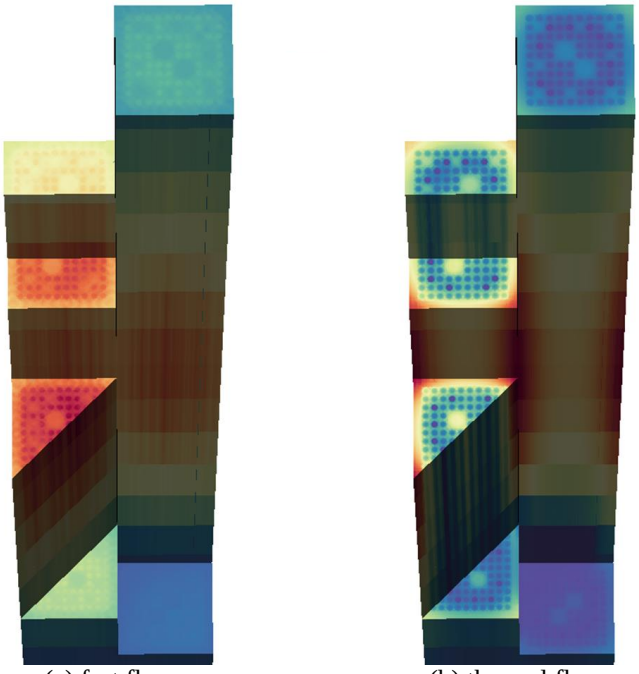

(a) fast flux (b) thermal flux

Fig. 9. Fast Flux (left) and Thermal Flux (right) for 3-D control cell.

The model was simulated at hot zero power conditions. The model had an MOC discretization of 0.05 cm ray spacing, 16 azimuthal angles and 2 polar angles per octant

using the Chebyshev-Yamamoto quadrature. The scattering treatment was TCP0 and the 47-group library was used. The model was discretized into 6-inch nodes axially for a total of 42 planes. The simulation was run in parallel on the Flux cluster at the University of Michigan using 42 processors for full spatial decomposition. The total run time of the simulation was 4 minutes and 13 seconds. The convergence criteria for the eigenvalue and flux were set to 5.0e-5 and these criteria were reached after 9 iterations.

2. 2-D BWR Full Core

The Peach Bottom cycle 1 loading pattern is shown in Fig. 10. The lattices are shown in Fig. 6. The core was modeled as 2-D at cold zero power with all rods out and no radial reflector. The cycle one loading patter is asymmetric which leads to the corresponding asymmetric power distribution shown in Fig. 11. In this model the MOC discretization used was 0.05 cm ray spacing, and 16 azimuthal and 2 polar angles per octant with the Cheybyshev-Yamamoto angular quadrature. The scattering treatment used was TCP0. The problem was run in parallel on the Falcon cluster at INL using 764 processors, one process for each assembly, for full spatial decomposition. The total run time of the simulation was 2 minutes and 29 seconds. The convergence criteria for the eigenvalue and flux were set to 1.0e-6 and these criteria were reached after 29 iterations.

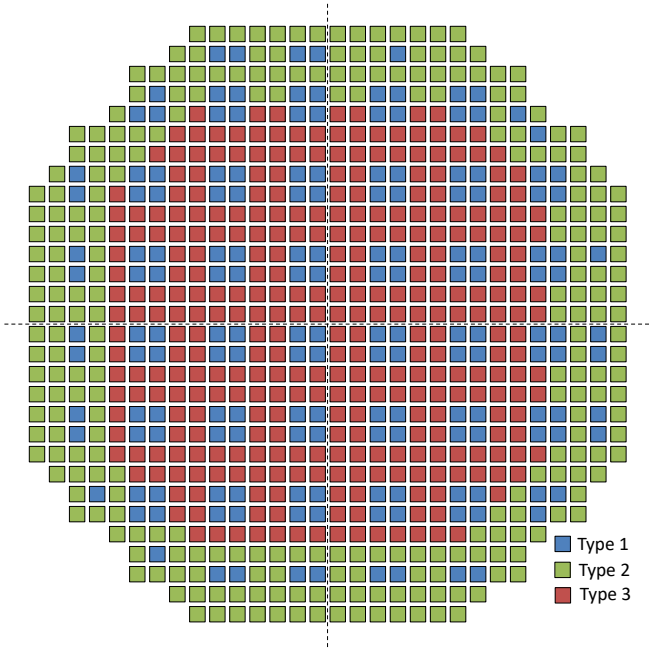

Fig. 10. Peach Bottom Unit 2 Cycle 1 loading pattern

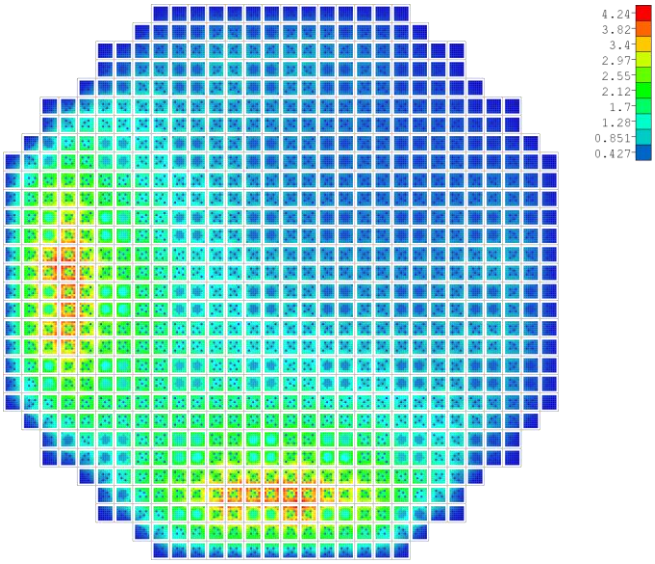

Fig. 11. Power distribution for 2-D Peach Bottom Unit 2 Cycle 1 CZP with all rods out.

V. CONCLUSIONS

The new BWR modeling capability within MPACT has been demonstrated for the Peach Bottom Unit 2 lattices and comparisons were made with reference KENO results. The comparison between MPACT and KENO shows good agreement.

Some results from demonstration problems were also shown. These results indicate that MPACT should be able to eventually scale to full core models.

Future work will focus on improving cross section needs for BWR at operating conditions, improving modeling for additional components like detectors, the shroud, and grid spacers. The capability to model additional bundle designs such as the GE9, GE11, ATRIUM 10, and SVEA is also planned. Longer term efforts will focus on coupling with COBRA-TF to be able to solve BWR problems with VERA-CS at hot full power conditions.

ACKNOWLEDGMENTS

This research was supported by the Consortium for Advanced Simulation of Light Water Reactors (www.casl.gov), an Energy Innovation Hub (http://www.energy.gov/hubs) for Modeling and Simulation of Nuclear Reactors under U.S. Department of Energy Contract No. DE-AC05-00OR22725. This research also made use of the resources of the High Performance Computing Center at Idaho National Laboratory, which is supported by the Office of Nuclear Energy of the U.S. Department of Energy under Contract No. DE-AC07-05ID14517.

REFERENCES

1. B. Kochunas, et al., "Overview of Development and Design of MPACT: Michigan Parallel Characteristics Transport Code," Proc. Int. Conf. M&C 2013, ANS, Sun Valley, ID, USA. May 5-9 (2013).
2. B. Kochunas, et al., "VERA Core Simulator Methodology for PWR Cycle Depletion," *Nucl Sci. Eng.*, **185**, 1, pp. 217-231, January 2017.
3. "Consortium for Advanced Simulation of Light Water Reactors (CASL)," http://www.casl.gov, (2016).
4. SCALE: A Modular Code System for Performing Standardized Computer Analyses for Licensing Evaluation, ORNL-TM/2005/39, Version 6, Vols. I–III, Oak Ridge National Laboratory, Oak Ridge, Tenn. (2009). (Available from Radiation Safety Information Computational Center at Oak Ridge National Laboratory as CCC-750.)
5. J. Askew, "A Characteristics Formulation of the Neutron Transport Equation in Complicated Geometries," Tech. Rep. AEEW-R-1108, United Kingdom Atomic Energy Authority (1972).
6. N.H. Larsen, "Core Design and Operating Data for Cycles 1 and 2 of Peach Bottom 2," EPRI Technical Report, NP-563, June, (1978).
7. D. Eberly, "The Minimal Cycle Basis for a Planar Graph," Geometric Tools, http://www.geometrictools.com/Documentation/MinimalCycleBasis.pdf, May 14, (2014).
8. W. Schroeder, K. Martin, and B. Lorensen, The Visualization Toolkit (4th ed.), Kitware, ISBN: 978-1-930934-19-1, (2006).
9. H. Childs, et al., "VisIt: An End-User Tool for Visualizing and Analyzing Very Large Data," High Performance Visualization--Enabling Extreme-Scale Scientific Insight, pp 357-372. (2012).
10. D. F. Watson, "Computing the n-dimensional Delauney tesselation with application to Voronoi polytopes," *Computer Journal*, **24**(2), pp. 167-172. http://dx.doi.org/10.1093/comjnl/24.2.167 (1981).
11. K.S. Kim, et al., "Development of the V4.2m5 and V5.0m0 Multigroup Cross Section Libraries for MPACT for PWR and BWR," CASL Technical Report, CASL-U-2017-1280-000, Feb. 14, (2017).
12. A. Godfrey, "MPACT Testing and Benchmarking Results," CASL Technical Report: CASL-U-2014-0045-000, http://www.casl.gov/docs/CASL-U-2014-0045-000.pdf, March 31, (2014).
13. "Physics of Plutonium Fuels BWR MOX Benchmark Specification and Results," NEA/NSC, Volume VII, ISBN: 92-64-19905-5, January (2003).